Propellant Condensation on Surfaces near an Electric Rocket Exhaust

THAINE W. REYNOLDS* AND EDWARD A. RICHLEY†
NASA Lewis Research Center, Cleveland, Ohio

The problem of neutral propellant atom fluxes arriving at surfaces situated near the exhaust of ion thrusters is considered. The problem is of interest because, for interplanetary missions, the combination of long thrusting times and low surface temperatures may allow ample opportunity for the buildup of an adsorbed layer of propellant. Both the thermal and electrical behavior of solar panel arrays, for example, could be affected by such a layer. Even spacecraft component surfaces outside a line-of-sight to the thruster exhaust may receive propellant impingement through reflection or re-evaporation from primary surfaces. Some simplified calculations of arrival rates are presented that allow accurate estimates to be made of the possible problem for a given spacecraft design. A specific case of a Jupiter flyby mission (from a recent Jet Propulsion Laboratory study) is evaluated in more detail. It is shown that condensation could occur on panels during the latter third of the thrusting period.

Introduction

IN the design of a solar-electric spacecraft, some unique problems can arise. One particular area of concern is that of determining the effects of thruster propellant exhaust on various spacecraft components, such as solar cell panels, power conditioning units, telemetry gear, or other instrumentation. At first thought it may appear that the entire problem is easily avoided by simply locating the thrusters on the spacecraft in such a way that no thruster exhaust has a direct line-of-sight to any spacecraft components. However, constraints imposed by packaging and deployment requirements may make this design approach impractical.

Exhausts from electrostatic thrusters consist of the highly energetic charged particles of the ion beam, lower energy charge-exchange ions, and low-energy neutral particles (Fig. 1). The latter are the result of thruster inefficiencies. Each type of thruster efflux presents a different interaction problem potential.

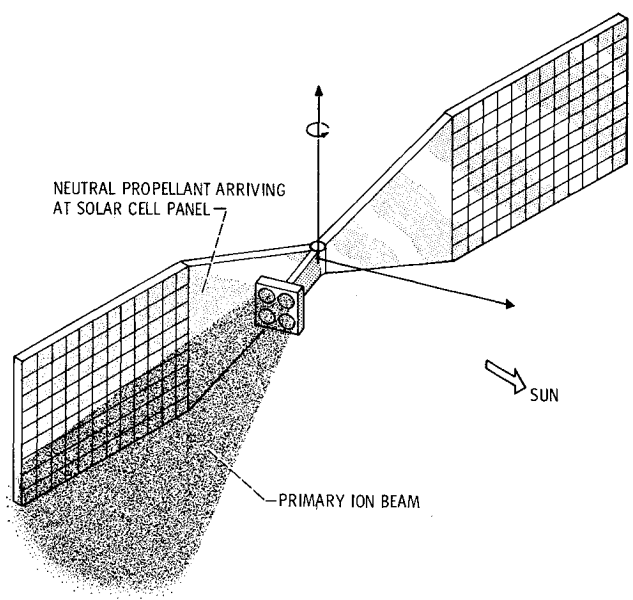

Fig. 1 Solar-electric spacecraft.

The high-energy particles are capable of causing severe erosion of objects in their path. Clearly, this type of encounter must be avoided. Fortunately, in most electric thruster types, the high-energy exhaust particles are reasonably well collimated. For example, it has been determined from a study of exhaust beam profile maps from several mercury ion thrusters at Lewis Research Center[1] that over 96% of the primary ion beam is confined within a beam spreading half-angle of 20° (Fig. 2). Thus, most interactions of this kind can be avoided by simply designing the spacecraft to permit a clear exhaust area for the main beam over these spreading angles.

Charge exchange ions formed in the exhaust beam are not collimated and their scattering and impaction on surrounding surfaces could be a problem. However, both the quantity and energy levels are considerably less than those of the primary ions.[2]

Because of the magnitude of neutral efflux and the lack of collimation, neutral particle effluxes present a potentially more serious problem. These particles leave the thruster with essentially a cosine distribution and some will arrive at and become deposited upon any component surface located downstream of the thruster exhaust plane. Furthermore,

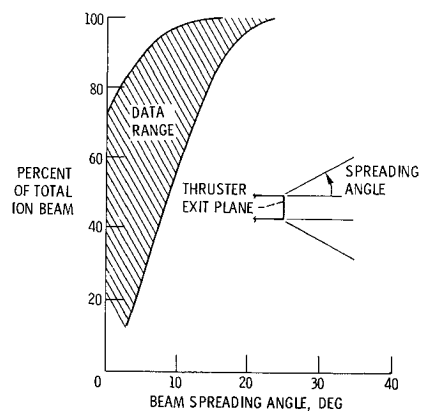

Fig. 2 Summary of mercury ion beam profile surveys. Data range covers several thruster sizes and operating conditions.

Presented as Paper 69-270 at the AIAA 7th Electric Propulsion Conference, Williamsburg, Va., March 3–5, 1969; submitted March 19, 1969; revision received July 15, 1969.

* Aerospace Research Engineer.
† Chief, Ion Physics Branch. Member AIAA.

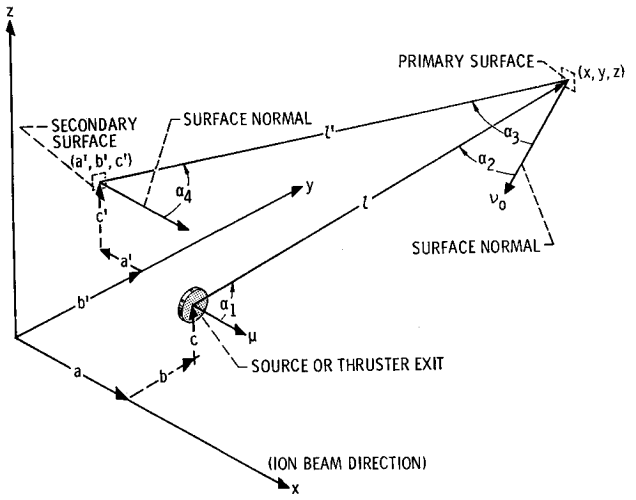

Fig. 3 Coordinate system schematic.

these particles will also be reflected or reevaporated from such downstream surfaces and some may arrive at spacecraft component surfaces upstream of the thruster exhaust plane—surfaces that are otherwise free from any primary particle impingement.

If under the thermal conditions of the surface, the arrival (or condensation) rates exceed the possible desorption rates, component performance might be seriously affected by cumulative propellant deposits. For example, metallic propellants such as cesium, mercury, or lithium may result in degradation of performance of solar cell arrays due to effects on optical properties or electrical failures. If rapid chemical reaction between the propellant and surface are possible, then deleterious effects might occur even without cumulative condensation. It is possible that monolayer coverage of the propellant gas on the surface may be reached relatively quickly, but subsequent layers will not build up. It is therefore of some consequence to know whether the phenomena associated with the adsorbing species and a particular surface is of importance at monolayer concentrations. Many surface properties, such as work function, ion emission rate, surface diffusion, catalytic reactions, and electrical conductivity, to name a few, are strongly affected by such low-level concentrations. Other properties, such as light transmission or thermal emittance also may be affected at low-level surface concentrations.

Each design of a spacecraft may require a specific calculation of the possible propellant impingement rates. However, some simple general calculations may quickly show whether the magnitude of the impingement is sufficient to warrant more detailed consideration. Similarly, the relations involved in the determination of surface coverage are relatively simple and general calculations involving these parameters may be made. Detailed calculations pertaining to a particular application, thus, may not be necessary.

With these thoughts in mind, this paper presents: 1) general calculations of particle arrival rates at planes located downstream of a source, 2) calculations of reflected or reevaporated particle flux back toward the source (or thruster) plane, 3) desorption rates of adsorbed gas layers in terms of desorption energies and surface temperatures, 4) an illustration of an application of the general calculations to a specific situation—a Jupiter flyby mission.[3]

To date, only a few studies dealing with expected impingement rates of propellant upon surfaces of a spacecraft have appeared in the literature. Backflow from high-pressure gaseous jet exhausts has been considered.[4,5] The potential problem with respect to ion beams has been recognized.[2,6] The specific effects of such impingement rates on particular surfaces is the subject of other investigations.[6] Finally, experimental determination of the possible effects of mercury contamination on solar panel arrays is planned for a forthcoming space electric rocket test (SERT) flight.[7]

Analysis

The process of condensate formation on a surface is a competition between the rate at which particles arrive and stick, and the rate at which they can leave the surface. That is $d\sigma/dt = \mu S - \nu$, where μ is the arrival rate, particles/cm²-sec; ν is the desorption rate, particles/cm²-sec; σ is the surface concentration of adsorbed species, atoms/cm²; S is the sticking coefficient.

The arrival rate μ depends upon the strength of the source of particles, the distance of the surface from the source, and upon the orientation of the surface with respect to the direction of the incoming particles. Arrival rates thus depend on geometrical relationships as well as the factors governing the strength of the source of particle emission. In the flux calculations herein, free-molecule flow conditions are assumed to prevail. The sticking coefficient is assumed to be unity for convenience. However, for any situation where it is not unity, it may be easily carried along in the calculations.

The desorption rate ν depends most strongly upon the temperature of the surface and the desorption energy—the strength of the bond between the adsorbed particles and the surface. (If the "surface" happens to be the same material as the absorbing gas, the desorption energy is the familiar sublimation energy.) The desorption energy of a gas from some surfaces may be considerably higher than the sublimation energy of the gas.

Arrival Rates

The coordinate system that is used in this analysis is shown in Fig. 3. In general, the particle source may be located arbitrarily at point (a,b,c). The primary surface of interest upon which particles may condense is located at point (x,y,z) downstream of the exit plane of the thrusters. Surfaces upstream of the exit plane of the thruster may also be impinged upon, and these surfaces will be referred to as secondary surfaces.

Primary surfaces

The ratio of the arrival rate μ at a surface of particles emitted at a rate ν from a point source emitting diffusely under conditions of free molecule flow is given by[8]

$$\mu/\nu = (\cos\alpha_1)(\cos\alpha_2)/l^2 \qquad (1)$$

The distance l in Eq. (1) has been nondimensionalized with respect to the thruster (source) radius. Equation (1) is a point source relation; however, it is readily shown that it yields fluxes that are within 5% of the more exact disk source relation at locations as close as five source radii away.[9]

In view of the uncertainty of the orientation of the deposition plane for any specific configuration, one may first calculate a maximum arrival rate at the (x,y,z) point. This would be the case for a surface oriented normal to the direction of particle flow (i.e., $\cos\alpha_2 = 1.0$). Some typical values of the maximum expected arrival rate ratios, calculated from Eq. (1), are shown in Fig. 4 for varying distances l and angles

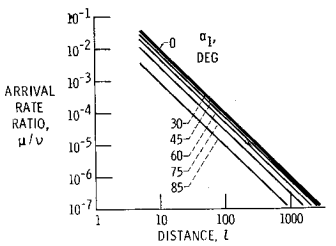

Fig. 4 Maximum expected arrival rate on surface downstream of source.

α_1. Notice that even for an α_1 of 85°, the magnitude of the μ/ν ratio is greater than 10^{-5} for distances up to 100, and at $l = 100$, the μ/ν ratio for $\alpha_1 = 85°$ is only one order of magnitude less than the value for $\alpha_1 = 0°$. The value of 10^{-5} will be shown later to represent a significant neutral flux. Of course, if there is more than one source of particle flux to a particular surface (i.e., more than one thruster) then values of μ from each must be determined and the values summed. The μ/ν values from Fig. 4 cannot be summed directly unless the source emission rates ν are all equal. Under the assumptions of free-molecule flow, no interaction between the neutral effluxes from the separate sources would be anticipated.

If, by means of the preceding calculation procedure, the maximum expected arrival rate at any point in question on the spacecraft is clearly too small to be of consequence to the particular spacecraft design, then a more accurate calculation of the flux ratio is unnecessary. If, on the other hand, additional calculations are indicated because of the magnitudes being significant, then the additional geometric factor $\cos\alpha_2$ for the specific orientation must be accounted for for each thruster and applied to the values in Fig. 4. This will be done for the illustrative problem presented later.

Secondary surfaces

The values of return flux ratios can be estimated using the coordinate system shown in Fig. 3. As shown in Fig. 3, we arbitrarily place the secondary surface of interest at (a',b',c'). The ratio of the arrival rate at (a',b',c'), via (x,y,z), to the source efflux at (a,b,c), is derived through the product of the following readily obtainable ratios,

$$\mu'/\nu = (\mu/\nu)(\mu'/\nu_0)(\nu_0/\mu) \tag{2}$$

where μ' is arrival rate at the surface at (a',b',c'); ν_0 is the leaving rate from the surface at (x,y,z); μ,ν are as previously defined. If we assume that condensation on the (x,y,z) surface is not occurring, or that equilibrium has been reached, then all the flux that arrives there will leave (i.e., $\mu = \nu_0$). In this case, Eq. (2) becomes

$$\frac{\mu'}{\nu} = \frac{\cos\alpha_1 \cos\alpha_2}{l^2} \frac{\cos\alpha_3 \cos\alpha_4}{(l')^2} r^2 \tag{3}$$

The factor r^2 appears in Eq. (3) because the "view" factor for the returning flux ratio μ'/ν_0 must be based on the reflecting surface area, but the dimensionless distances l and l' have been defined in terms of the source (thruster) radius. Therefore r is a radius of an emitting area on the reflecting surface, nondimensionalized to the thruster radius.

As before, a maximum relative flux ratio from (x,y,z) to (a',b',c') is obtained for an (a',b',c') orientation perpendicular to l' (that is, when $\cos\alpha_4 = 1.0$). To illustrate the calculation of the flux ratio μ'/ν at some specific secondary surface location, we choose arbitrarily here a point located back at the source center $l(= l')$. Flux at this location will be representative for surfaces near the thruster plane, but outside a region subject to direct impingement. There will be a maximum back flux at that point for the conditions $\cos\alpha_2 = \cos\alpha_3 = \cos\alpha_4 = 1.0$, so that the return flux is simply

$$\mu'/\nu = (\cos\alpha_1) r^2/l^4 \tag{4}$$

Some representative values of maximum return flux ratios from Eq. (4) are shown in Fig. 5 for $r = 1$, that is, for a reflecting area equal to the thruster area.

Clearly, Eq. (4) differs from Eq. (1) simply by the factor r^2/l^2; however, it is interesting to note that even for an α_1 of 85° the magnitude of the return flux ratio is greater than 10^{-5} for distances up to 10 thruster radii. Significant neutral flux is indicated for this value of 10^{-5} as will be shown later. Again, if there is more than one thruster or more than one reflecting surface (or a larger reflecting surface) that can contribute to return flux, the values of μ' must be determined for each and added to obtain the total, true returning arrival rate. If this estimated maximum appears significant to the particular application, more refined calculations are indicated.

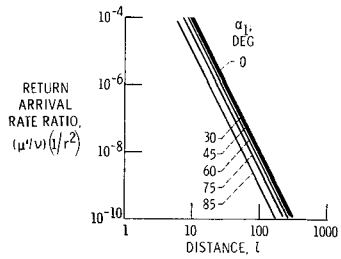

Fig. 5 Maximum expected return arrival rates to surfaces near thruster exit plane.

Table 1 Properties of various materials

Material	Density-to-mass ratio, ρ/M, g-mol/cm³	Desorption energy, E_{des}, ev	Monolayer surface concentration, $\sigma_m \times 10^{-15}$, No./cm²
Ag	0.0974	2.96	1.52
Al	0.0997	3.36	1.54
Cs	0.0141	0.81	0.422
Hg	0.0701	0.63	1.22
Li	0.0770	1.65	1.30
Mg	0.0714	1.52	1.24
Mo	0.1060	6.87	1.61
Na	0.0422	1.13	0.86
Ni	0.1510	4.43	2.04
Ta	0.0893	8.10	1.43
U	0.0795	5.07	1.33
W	0.1040	8.75	1.58

Desorption Rates

The desorption rate of particles from a surface is usually described by the relation[10]

$$\nu = \sigma e^{-(E_{des}\, kT_s)}/\tau_0 \tag{5}$$

where ν is desorption rate, particles/(cm)²(sec); τ_0 is a constant, 10^{-13} sec; E_{des} is desorption energy, ev/atom; T_s is surface temperature, °K; k is Boltzmann constant; σ is surface concentration, particles/cm². Desorption rates for fractional monolayer coverages are discussed in Ref. 11. In the present application we shall concern ourselves primarily with desorption rates for monolayer coverage. The value of σ_m (surface concentration for a monolayer coverage) for a material depends on the crystal face involved, but to the accuracy required in the present situation we can use the $\frac{2}{3}$ root of the number density of the solid as a good approximation to the surface density,

$$\sigma_m \cong (6.023 \times 10^{23}\, \rho/M)^{2/3} = 7.15 \times 10^{15}\, (\rho/M)^{2/3} \tag{6}$$

where ρ is the density of solid, g/cm³; M is mass in atomic mass units. Equation (5) thus reduces to

$$\nu = 7.15 \times 10^{28}\, (\rho/M)^{2/3} e^{-E_{des}/kT_s} \tag{7}$$

Values of ρ/M and E_{des} (heat of sublimation in these cases[12]) for a number of materials are shown in Table 1 and desorption rates calculated according to Eq. (7) are shown in Fig. 6. Data for a number of materials from Table 1 are shown therein also. Values of desorption rate of a material from Fig. 6 are used in the illustrative example presented later to compare with calculated arrival rates to determine whether condensation conditions exist at a particular surface. The values of ν used are in close agreement with values calculated from vapor pressure data over the range of interest.

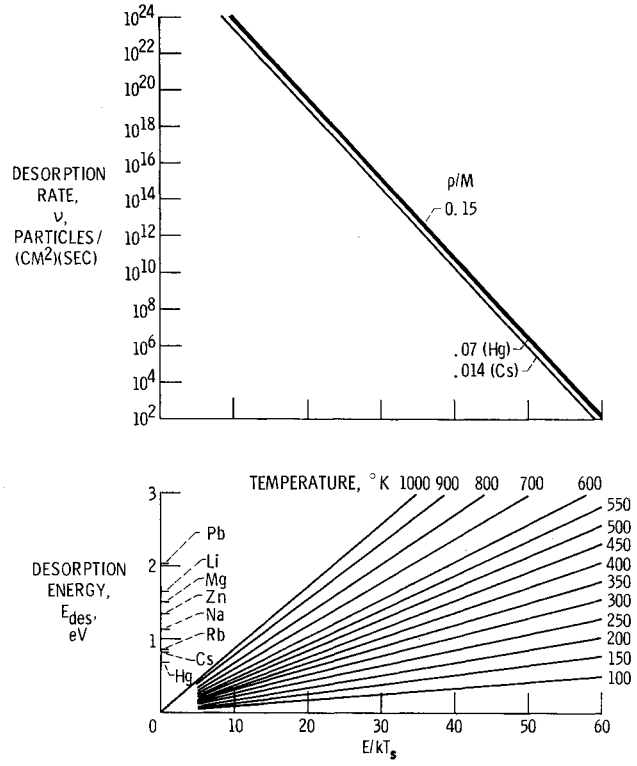

Fig. 6 Desorption rate from monolayer or more concentration as function of temperature, energy, and surface density.

Discussion and Illustrative Problem

The first assumption made here is that, as portrayed in Fig. 1, the spacecraft configuration will at some time require the location of a surface downstream of the plane of the thruster exhaust (otherwise no problem exists). Our objective is to find out if the rate of propellant impingement on that surface is high enough to create any problems on that surface, or for other surfaces by reflecting propellant back toward them.

The neutral atom emission rate for an electric thruster is readily calculated from

$$n_a = \frac{J}{q}\left(\frac{1-\eta}{\eta}\right) \times 10^{-4} = \frac{I}{(\pi r^2)q}\left(\frac{1-\eta}{\eta}\right) \times 10^{-4} \quad (8)$$

where I is the ion beam current, amp; J is the ion beam current density, amp/m²; r is the thruster radius, m; q is the electron charge, 1.6×10^{-19} coulomb/particle; η is the propellant utilization efficiency, the fraction of total propellant flow which is ionized.

Thus, for example, a bombardment thruster with a 30 amp/m² beam and a 90% propellant utilization efficiency would have a neutral atom emission rate n_a of 2.2×10^{15} atoms/(cm²)(sec).

Then, using Fig. 4, we can note that arrival rates at $l = 10$, for example, may be as high as 2.2×10^{12} to 2.2×10^{13} atoms/(cm²)(sec). With mercury as the propellant, this arrival flux represents possible condensation rates (depending on component temperatures) of 0.002 to 0.02 monolayers per second, or from 170 to 1700 monolayers per day. Not only is this situation a possible troublesome one, but also, with any sizable surface area so exposed to this neutral flux, the return flux to areas behind the thruster plane could also be of concern. From Fig. 5 we note that for the same distance, $l = 10$, the return flux ratio is 10^{-5} to 10^{-4}. Thus, even from a reflecting area only as large as the thruster area (i.e., $r = 1$), the possible return flux rates from this distance would be equivalent to from 2 to 20 monolayers per day. From larger reflecting areas, and with more than one thruster operating, this return flux would be proportionately greater. More detailed calculations would be required depending on the spacecraft design and mission profile.

One such mission requiring more careful analysis is the Jupiter flyby mission (JFB).[3] A schematic of one spacecraft design from Ref. 3 is reproduced here in Fig. 7. The spacecraft has solar panels that extend to about a 15-m radius and which can pivot about the z axis, extending out downstream of the thruster plane. The craft would be used for a direct trajectory flyby and have a total thrusting time of 470 days. Thrust would be obtained from four 2.5 kw mercury bombardment thrusters.

For this illustrative problem we have chosen a coordinate system suggested by the general characteristics of the JFB spacecraft (see Figs. 7 and 8). The coordinate system is similar to that shown in Fig. 3 with the added stipulation that the surfaces at which the arrival fluxes are calculated are the solar panel surfaces which rotate about the z axis. Also, the coordinates of a point on that surface are given in terms of their Y, Z, values when the panel is at $\beta = 0°$ angle (i.e., when the solar panel is parallel to the thruster exit plane). With this definition the angle β is equal to the thrust angle Γ, as used in Ref. 3. The thrust angle is the angle between the thrust vector and the sun line to the spacecraft.

With this specification on the problem, the flux at any point on the solar panel from one thruster located at (a,b,c) is given by the following relation derived from Eq. (1):

$$\frac{\mu}{\nu} = \frac{(y_0 \sin\beta - a)(a\cos\beta - b\sin\beta)}{[(y_0\sin\beta - a)^2 + (y_0\cos\beta - b)^2 + (z_0 - c)^2]^2} \quad (9)$$

A negative value of flux ratio from this equation means that the particles are striking the back side of the array. This will be the case for $\beta > \tan^{-1}(a/b)$.

Values of the arrival rate ratio from Eq. (9) were calculated, with the aid of a digital computer, for various combinations of the thruster location (a,b,c), panel point (x,y,z), and panel angle β. In using Eq. (9), all distance variables were nondimensionalized in terms of the thruster radius.

Calculated values of μ/ν along three rays shown in the first quadrant in Fig. 7 are plotted in Fig. 9. The μ/ν plotted is the total value from four thrusters which, for convenience were located at $a = 2$, $b = \pm 2$, and $c = \pm 2$. (For the actual JFB configuration, $a = 7.67$.) Two representative

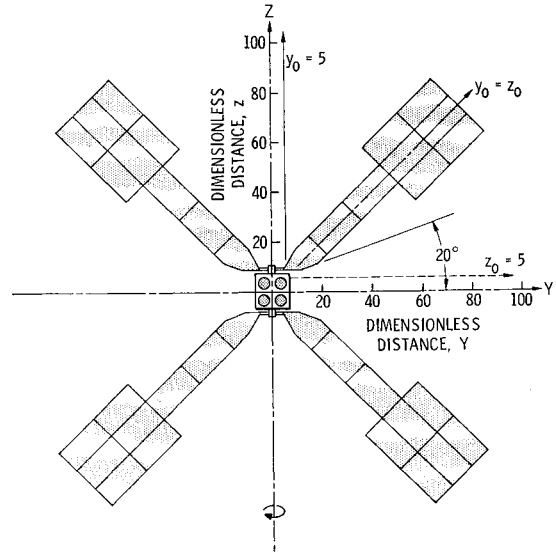

Fig. 7 View of JFB spacecraft facing solar panel array. Array rotates about z axis.

Table 2 Optical properties used for calculations

Hg on solar panels	Total hemispherical emittance: Sun side, ϵ_f	Total hemispherical emittance: Backside, ϵ_b	Solar absorptance, α_f	Ratio, $\frac{\alpha_f}{\epsilon_f + \epsilon_b}$
None	0.89–0.93	0.93–0.96	0.72–0.86	0.38–0.47
Front surface	0.10	0.93–0.96	0.22	0.21
Back surface	0.89–0.93	0.10	0.72–0.86	0.82
Both surfaces	0.10	0.10	0.22	1.1

orientations of the panel, $\beta = 30°$ and $\beta = 75°$, are shown. Since the total neutral emission rate ν from the four thrusters is equivalent to about 6.3×10^5 monolayers per day, flux ratios of 10^{-5} in Fig. 9 are comparable to 6.3 monolayers per day impingement rates.

The diagonal ray is subject to impingement rates of several monolayers per day even out to 40 or 50 thruster radii away. A surface situated at most any location in the quadrant would be susceptible to considerable impingement within 20 thruster radii of the source.

A plot of the flux (monolayers per day) along the diagonal axis of the panel is shown in Fig. 10 for several angular orientations. Because of the spacecraft configuration and sun orientation, at panel angles between 45° and 135°, the flux to the sun side comes from only two thrusters. At these angles, neutral efflux from the other two thrusters impinges on the back side of the panel. By virtue of symmetry, arrival rates on the sun side at a given angle β are identical to those on the back side at an angle $180°-\beta$.

As can be seen from Fig. 10, the impingement rates are strongly dependent on the distance from the thrusters. But, the point to be emphasized here is simply that even outside the cone angle of the main ion beam, considerable propellant atom flow can arrive at structural surfaces which lie downstream of the thruster exit plane. Whether the magnitude of this arrival rate of propellant is sufficient to cause any operational problems for that surface is another question. However, one can calculate whether or not the propellant will condense and build up a covering layer on the panels. To estimate this situation it is necessary to consider the several factors controlling the solar panel temperature.

The equilibrium temperature of a panel at any location in space is calculated from a radiation heat balance,

$$Q_E(\alpha_f \cos\gamma)/R^2 = \sigma(\epsilon_f + \epsilon_b)T_p^4 \qquad (10)$$

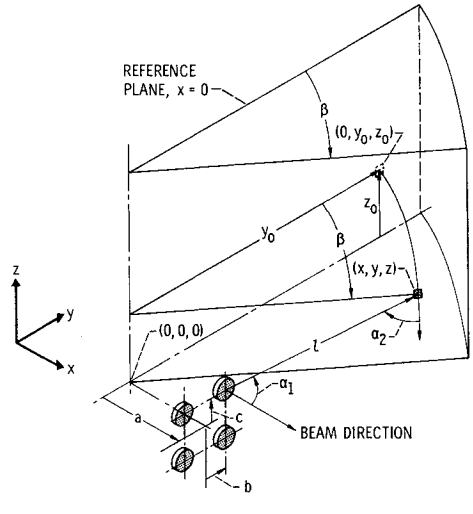

Fig. 8 Schematic of simulated JFB coordinate system.

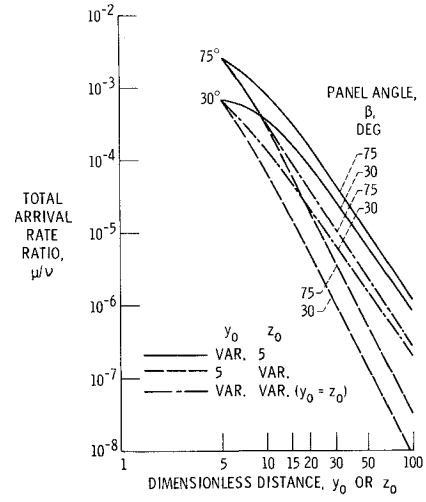

Fig. 9 Variation of total arrival rate ratio along three rays in first quadrant. Total from four thrusters.

or

$$T_p = \left[\frac{Q_E \cos\gamma}{R^2\sigma}\left(\frac{\alpha_f}{\epsilon_f + \epsilon_b}\right)\right]^{1/4} \qquad (11)$$

where Q_E is the solar constant at 1.0 a.u., 1393 w/m^2; R is the distance from sun, or range, a.u.; σ is the Stefan-Boltzmann constant, 5.73×10^{-8} w/(m^2)(°K^4); α_f is the solar absorptance of panel surface facing sun; ϵ_f,ϵ_b are the thermal emittance of front and back surfaces of panel, respectively; γ is the angle between surface normal and sun line.

The values of α_f, ϵ_f, and ϵ_b depend upon the nature of the surface, and whether or not it has condensate on it. (Recent experimental investigations have been undertaken at the Lewis Research Center to determine values for α and ϵ for thin-film solar cells[13,14].) The equilibrium temperature, T_p, from Eq. (11) is shown plotted in Fig. 11 for a range of $\alpha_f/(\epsilon_f + \epsilon_b)$ values, and for $\gamma = 0$, that is, a surface normal to the sun line. If the thermal properties of the surface do not change, the surface temperature falls inversely with the square root of the range.

For the JFB spacecraft, the mission profile discussed in Ref. 3 yields the time variation of variables pertinent to this condensation discussion shown in Figs. 12–14. These are the panel angle, the range, and the thruster propellant flow rate. The total neutral mercury arrival rate at any location

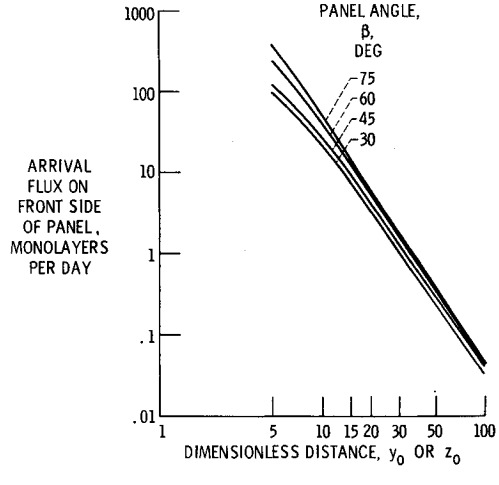

Fig. 10 Arrival rate along panel diagonal (front surface) for various angles. Four thrusters at $a, b, c = (2, \pm 2, \pm 2)$.

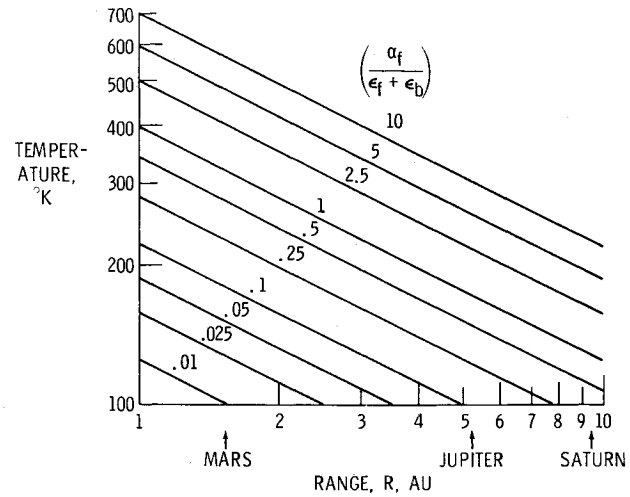

Fig. 11 Variation of equilibrium panel temperature with distance from sun for varying surface thermal properties.

on the solar panels for any time during the mission can be calculated through use of these curves and Eqs. (8) and (9). The solar panel temperature, necessary to estimate possible desorption rates from the panel via Eq. (5) or (7) can be obtained from Fig. 11. However, the α/ϵ ratio to use to determine the temperature will depend upon whether condensation can occur, since, in general, the condensate layer would be expected to have different thermal properties than the panel itself.

Some representative values of α and ϵ for clean surface solar cells[13,14] and for a mercury surface[6,15] are shown in Table 2, along with the resulting values of $\alpha_f/(\epsilon_f + \epsilon_b)$ for the various possible combinations of surfaces. Higher values of $\alpha_f/(\epsilon_f + \epsilon_b)$ result in higher equilibrium temperatures (Fig. 11) for any given heat input rate. Those combinations that have a higher value of $\alpha_f/(\epsilon_f + \epsilon_b)$ than that of the clean panels will, then, be self-cleaning in a sense. That is, any tendency of a deposit to form on surfaces in a way which would raise the $\alpha_f/(\epsilon_f + \epsilon_b)$ ratio would tend to raise the panel temperature. The resulting increased desorption rate would then tend to clean the panel of adsorbate. Such is the case in this illustration for mercury condensation on the back surface of the solar panel only, or on both front and back surfaces simultaneously. However, an essentially indeterminate situation may result for the case of mercury condensation on the front surface only. If a condensed layer is assumed on the front surface only, the resultant panel temperature may be such as to permit condensation, whereas, the temperature of a clean panel would be too high to permit condensation. Therefore, it is clear that the actual equilibrium conditions of the surface depend upon its previous history.

From a knowledge of the mercury arrival rate at a point on the panel and the desorption rate curve for mercury (Fig. 6), one can determine an equilibrium temperature (i.e., a temperature where $\mu = \nu$). For purpose of illustration here, these temperature levels so calculated for the arrival rates at three locations on the panel diagonal are shown in Fig. 15. Figure 15 is also a plot of a portion of Fig. 11. It shows two possible clean panel temperature curves determined from

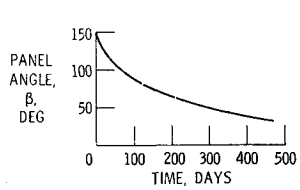

Fig. 12 Orientation of panel during thrust phase.

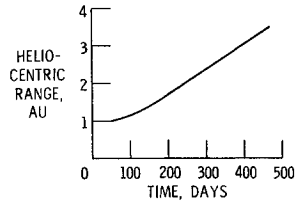

Fig. 13 Range of spacecraft during thrust phase.

the α, ϵ data of Ref. 13. The clean panel region indicates a band of possible temperatures which reflect the spread in experimentally determined optical properties. The other curve is for an *assumed* mercury coating on the same front surface. Whether condensation will occur on the panel depends on the applicable value of $\alpha_f/(\epsilon_f + \epsilon_b)$. If the panel temperature is on or below the calculated temperatures representing the equilibrium arrival rates, a condensate layer will build up at that position on the JFB panel.

The results shown in Fig. 15 should be examined carefully to fully understand their significance. For example, the 5,5 curve shows that, if the panel has a "clean" history, condensation should not occur at the 5,5 location on the panel until the spacecraft is at about 2.50 to 2.75 a.u. For the actual JFB configuration the solar cell panels begin at about a 16,16 location. From Fig. 15 it can be estimated that, for this location, condensation would occur at about 3 a.u.

Actually, at about 2 a.u., the flux levels and possible panel temperatures approach the condition of indeterminancy mentioned previously. Without a condensate layer present, the panel temperature would be expected to remain above the condensation level. However, if the panel temperature should be temporarily cooled below the condensation temperature, due to misorientation of the spacecraft, for example, the resulting value of the parameter, $\alpha_f/(\epsilon_f + \epsilon_b)$, would be such as to keep the panel temperature below the condensation level and the condensate layer would continue to grow. Thus, the importance of the panel temperature history during the mission is evident.

Return flux values are more difficult to evaluate in detail, but it may be noted that out to distances of 10 thruster radii, values of return flux ratio μ'/ν of up to 0.01 of the primary flux rates can be expected for reflecting surface areas of only about 0.05 m² (i.e., equal to the JFB thruster area). With the JFB array shown in Fig. 7, the total structure area exposed to primary flux within a distance of $l = 10$ will be several times this thruster area. Therefore, the return arrival rates near the thruster plane can be expected to be considerably more than 0.2 to 0.5 monolayers per day (see Fig. 9). Since these surfaces are likely to be colder than the solar panels, condensation on them is possible even sooner than on the solar panels themselves. Surface temperatures of around 180°K would permit a mercury condensate layer to grow at arrival rates exceeding one nonolayer per day.

Concluding Remarks

Consideration of the neutral atom efflux to be expected from the thrusters on electric spacecraft has led to the following general conclusions:

1) Neutral efflux rates are high enough and interplanetary flight times long enough that considerable total propellant

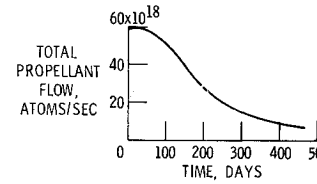

Fig. 14 Variation of total propellant flow rate during thrust phase.

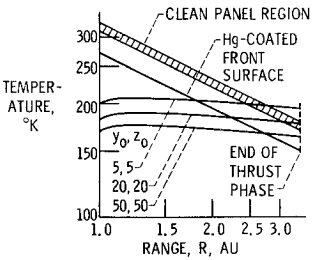

Fig. 15 Comparison of possible panel temperature and condensation temperature for JFB spacecraft during thrusting phase of mission.

can impinge on nearby spacecraft components located downstream of the thruster exhaust plane.

2) Even surfaces not in the line-of-sight of initial propellant atom trajectories may still receive impingement through reflection or reevaporation from surfaces in the direct line of sight of the thruster exhaust.

3) Accurate estimates of probable maximum neutral propellant arrival rates on surfaces of an electric spacecraft can be easily made using simplified molecular flow relations. The magnitude of these probable maximum rates can be reviewed in consideration with the planned mission profile to determine whether more detailed ad hoc calculations are required.

4) Mercury flux rates onto the solar panels of a proposed JFB spacecraft are such that propellant condensation on the portion of the panels close to the thruster may occur in the latter stages of the mission. Specifically this situation occurs when the spacecraft is at about 2.0 a.u. In time, the portions over which condensation can occur then extend outward away from the thrusters, up to and including the farthest most portions of the solar cell panels. More detailed calculations probably are in order.

5) The example problem illustrated the importance of the solar panel temperature history throughout the mission. It was shown that an unplanned premature cooling of the panel could upset the thermal equilibrium of the situation sufficiently to cause unexpected condensation to occur. The condensate might re-evaporate or condensation might then continue depending upon which surfaces were affected.

References

[1] Cohen, A. J., unpublished analysis, 1968, NASA.

[2] Staggs, J. F., Gula, W. P., and Kerslake, W. R., "Distribution of Neutral Atoms and Charge-Exchange Ions Downstream of an Ion Thruster," *Journal of Spacecraft and Rockets*, Vol. 5, No. 2, Feb. 1968, pp. 159–164.

[3] Barber, T. et al., "1975 Jupiter Flyby Mission Using a Solar Electric Spacecraft," Rept. ASD 760-18, March 1968, Jet Propulsion Lab., Pasadena, Calif.

[4] Noller, H. G., "Approximate Calculations of Expansion of Gas from Nozzles Into High Vacuum," *Journal of Vacuum Science and Technology*, Vol. 3, No. 4, July-Aug. 1966, pp. 202–207.

[5] Grier, N. T., "Back Flow from Jet Plumes into Vacuum," TN D-4978, 1968, NASA.

[6] Hall, D. F. et al., "Evaluation of Electric Propulsion Beam Divergence and Effects on Spacecraft," 2nd Quarterly Letter, Contract NAS7-575, Jan. 1968, TRW Systems Inc.

[7] Kerslake, W. R., Byers, D. C., and Staggs, J. F., "SERT II Experimental Thruster System," AIAA Paper 67-700, New York, 1967.

[8] Patterson, G. N., "A State-of-the-Art Survey of Some Aspects of the Mechanics of Rarefied Gases and Plasmas," Rept. ARL 64-60, 1964, Toronto Univ., Canada.

[9] Reynolds, T. W. and Richley, E. A., "Free-Molecule Flow and Surface Diffusion through Slots and Tubes—A Summary," TR R-255, 1967, NASA.

[10] DeBoer, J. H., "Adsorption Phenomena," *Advances in Catalysis*, Vol. 8, edited by W. G. Frankenberg, V. I. Komerewsky, and C. K. Rideal, Academic Press, New York, 1956, pp. 17–161.

[11] Reynolds, T. W., "Adsorption-Desorption Behavior of Homogeneous and Heterogeneous Metal Surfaces," TN D-4789, 1968, NASA.

[12] Honig, R. E., "Vapor Pressure Data for the Solid and Liquid Elements," *RCA Review*, Vol. 23, No. 4, Dec. 1962, pp. 567–586.

[13] Liebert, C. H. and Hibbard, R. R., "Theoretical Temperatures of Thin Film Solar Cells in Earth Orbit," TN D-4331, 1968, NASA.

[14] Jack, J. R. and Spisz, E. W., "Thermal Radiative and Electrical Properties of a Cadmium Sulfide Solar Cell at Low Solar Intensities and Temperatures," TN D-4818, 1968, NASA.

[15] Parker, W. J. and Abbott, G. L., "Theoretical and Experimental Studies of the Total Emittance of Metals," NASA SP-55, 1965, pp. 11–28.